Short Frame Transmission at Very Low SNR by Associating CCSK Modulation with NB-Code

Kassem Saied, Ali Chamas Al Ghouwayel, E. Boutillon

Short Frame Transmission at Very Low SNR by Associating CCSK Modulation with NB-Code

Kassem Saied, Ali Chamas Al Ghouwayel and Emmanuel Boutillon .

***Abstract*—In this paper, we present a frame structure that can be viewed as a preamble for the detection and synchronization process (leading to low cost receiver) and as an encoded codeword carrying the transmitted message (leading to reliable transmission). This duality facilitates an ALOHA protocol avoiding preamble overhead. The frame structure, named Quasi-Cyclic Short Packet (QCSP), is based on the association of a Cyclic Code Shift Keying (CCSK) modulation and a non-binary error control code. The detection/correction algorithm of the QCSP system is presented, its performance is theoretically derived and discussed for different parameters. A QCSP frame can be transmitted and received correctly with an error probability of 10^{-4}, distanced by 1.2 dB from Polyanskiy's bound (an estimated Shannon's limit for small packet size) at -11 dB of SNR for a payload of 360 bits. Compared to a classical preamble-based frame using a modern binary error control code, the size of a QCSP frame is reduced by 23%. Moreover, detecting a QCSP frame requires a lower complexity than detecting a longer classical preamble.**

***Index Terms*—Preamble-less Detection, QCSP, CCSK, NB-Code, AWGN, LPWAN.**

I. Introduction

Future standards of radio communications are expected to support the connections of over 50 billion devices by the next decade via the Internet of Things (IoT) and its protocols. This topic constitutes the center of interest in both academic and industrial sectors [1]. Given the constantly increasing number of connected devices, the design of the network carrying such IoT connections should be re-considered in order to support such massive connectivity.

In this context, various applications are supported by the utilization of a range of technologies. The performance oriented categories like LTE or WiFi represent the first edge of these technologies. Such categories deploy sophisticated concepts including multi-user Multi Input Multi Output (MIMO) to boost throughput and spectral efficiency. However the Low Power Wide Area Networks (LPWAN) form the other edge of the technologies [2]. The requirements of LPWAN include a large coverage area, low data rates, a small data packet size, low energy consumption at the device side [3]. EC-GSM [4], Narrow Band-IoT [5], LTE-M [6], LoRa [7], and SigFox [8] are examples of current IoT standards.

K. Saied is both with Lab-STICC (UMR 6285, CNRS), Université Bretagne Sud, Lorient, 56100 France and with computer and communication department, Lebanese International University, Beirut, Lebanon. Email: kassem.saied.lu@gmail.com.

A. Chamas Al Ghouwayel was with computer and communication department, Lebanese International University, Beirut, Lebanon. He is now with Efrei Paris, Villejuif, France. Email: ali.ghouwayel@efrei.fr.

E. Boutillon is with Lab-STICC (UMR 6285, CNRS), Université Bretagne Sud, Lorient, 56100 France. E-mail: emmanuel.boutillon@univ-ubs.fr.

At system level, reducing "meta-data" throughput, (i.e., the exchange of information linked to signaling, synchronization and identification) is the new paradigm of massive IoT networks [9]. Polyanskiy has shown in [10], that asynchronism, even with short packets, does not affect the capacity of the channel; this means that classical methods that use coordination for synchronization and collision avoiding are far from the optimum, since the energy used for coordination is simply wasted.

In an unslotted ALOHA protocol, the base station has no information regarding the time of arrival of messages (or frames). Moreover, in the context of the paper, each frame is assumed to be affected by a frequency offset. This frequency offset can be generated by clock-Jitter of a local device or Doppler effect. It can be also generated in a purpose for different motivations which are out of the scope of the paper (multi-users access for example). The problem of frame detection at low Signal to Noise Ratio (SNR), expressed along the paper as energy per symbol E_s/N_0, is examined in the literature. Many papers propose detection, frequency and time synchronization algorithms based on the transmission of a preamble heading each frame [11]–[15]. The classical preamble-based method allows to greatly simplify the receiver complexity thanks to known received information. However, the use of a preamble alleviates significant part of bandwidth resource when the message payload is small as shown in Fig. 11 in the results section.

The engineering literature has already examined and explored various preamble-less methods for short packets [16]–[20], but all the proposed algorithms have proved their efficiency on positive decibel SNR values (i.e., SNR $>$ 0 dB). In this paper, the authors propose to use the modulation presented in [21] to transmit short packets without any additional symbol that is dedicated to detection and synchronization working at ultra-low SNR, i.e., SNR $<$ 0 dB. This "preamble-less frame" is hereby referred to as a Quasi-Cyclic Short Packet (QCSP) frame. It is based on the use of a Cyclic Code Shift Keying (CCSK) modulation scheme [22] [23], characterized by an inherent correlation property that will help the frame detection and synchronization at the receiver side. The key idea is to consider the whole frame first as a preamble for detection and timing synchronization, then as an encoded payload for error correction decoding and information recovery. This idea is implemented thanks to the cyclic property of the CCSK modulation. It allows the design of efficient detection and synchronization algorithms based on the correlation of the received frame with cyclically shifted versions of a predefined pseudo random sequence. In addition, this CCSK modulation

is jointly designed with powerful Non-Binary (NB) forward error correction codes defined over a Galois Field GF(q), where $q > 2$, such as NB-Low Density Parity Check (NB-LDPC) Codes [24], NB-Turbo [25], NB Turbo Product Codes [26], and NB-Polar codes [27]. These codes benefit first from good error-correcting performance, and furthermore, due to their non-binary nature, they enables a direct mapping between codeword symbols and the points of a high order modulation [28]. In this paper and without loss of generality, the NB-LDPC is considered as the NB-code.

The main contribution of this paper is the proposition of a practical detection algorithm of a QCSP frame in the Additive White Gaussian Noise (AWGN) channel that does not require any prior knowledge of the time of arrival and the frequency offset. Using the tools of detection theory, the paper derives the mathematical equations to express the probability of miss-detection and the probability of false alarm according to the QCSP structure and the channel conditions. The detection performance of the proposed system is assessed depending on the different QCSP system parameters. In addition, this work gives insights on the joint transmission performance (detection and correction probabilities) that could be obtained with a QCSP frame. This work is conducted in the context of wireless sensor networks, where low-cost sensors are considered. The system is an unsynchronized ALOHA protocol with potential carrier-frequency offset, or Doppler effect. Typical applications can be found in the Industrial, Scientific and Medical (ISM) band (as for the LoRa and SigFox protocols) of communication with low earth orbiter satellites. Note that a QCSP frame could also be used in more structured networks, which is not the main objective of the paper.

The rest of the paper is organized as follows. Section II introduces the system model and the detection problem. Section III describes in details the detection method and the main detection metric, called score function. Sections IV derives a theoretical model of the proposed detection algorithm and validates it through Monte-Carlo (MC) simulations over a complex AWGN channel. Section V discusses the effect of different parameters that affect the CCSK-based system. Then, a detection-correction approach is analyzed, based on the performance obtained and the estimated Shannon limit for small packet sizes defined by Polyanskiy [29]. A practical example is also given where the NB-LDPC is used as a decoder in the QCSP system, and the obtained result is finally compared to a classical Zadoff-Chu preamble-based frame [30] [31], using the LDPC (proposed in 3GPP (5G) standard) as an error control code. Finally, section VI concludes the paper.

II. System Model

In this section, we present the principle of a CCSK modulation in the context of its association with NB-codes, and the system model being considered. We present the effect of the channel at the receiver side when neither time nor frequency information is available. After that, we illustrate how the time-frequency space will be decomposed in the QCSP system. Finally, we define the detection problem based on signal detection theory. Fig. 1 shows the system model of the communication link being considered.

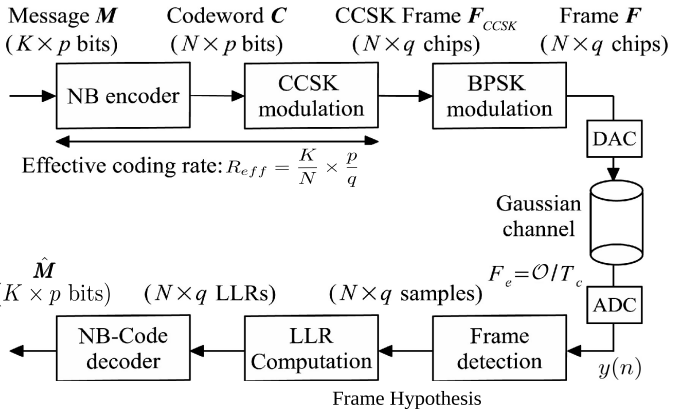

Fig. 1: CCSK-based System Model

A. Transmitter side

We consider a NB code defined over the Galois field with q elements, denoted by GF(q). Each GF symbol can be coded by $p = \log_2(q)$ bits, and thus can be represented by an integer number between $[0, 2^p - 1]$. The input of the NB-code is a binary message $\boldsymbol{M}$ of size $m = K \times p$ information bits, or equivalently, K GF(q) symbols. The NB-encoder generates a codeword $\boldsymbol{C}$ of N GF(q) symbols, i.e., the codeword $\boldsymbol{C}$ is represented as

$$\boldsymbol{C} = [c_0, c_1, \ldots, c_{N-1}], \text{ with } c_k \in \mathrm{GF}(q),\ k = 0, 1, \ldots, N-1. \tag{1}$$

The code rate is $R_c = K/N$.

The CCSK modulation uses a pseudo-random binary sequence $\boldsymbol{P}_0 = \{P_0(i)\}_{i=0,\ldots,q-1}$ of length q with good auto-correlation properties, where $P_0(i) \in \{-1, 1\}$. The circular auto-correlation function $\theta(j)$ of a sequence $\boldsymbol{P}_0$ is defined as

$$\theta(j) = \sum_{i=0}^{q-1} P_0(i) P_0(i+j \bmod q), \quad \forall j = 0, 1, \ldots, q-1. \tag{2}$$

Thus, an ideal auto-correlation function verifies $\theta(0) = q$ and should verify $\theta(j) = 0, \forall j = 1, 2, \ldots, q-1$. In practice, except for particular cases, no known solution exists and the quality of a $\boldsymbol{P}_0$ sequence can be measured on how the partial auto-correlation vector $(\theta(1), \theta(2), \ldots, \theta(q-1))$ is close to the zero vector. The norm we used to measure this distance is the ℓ_2-norm, where $\ell_2(\theta) = \sum_{j=1}^{q-1} \theta(j)^2$. A Genetic algorithm has been used to construct sequence $\boldsymbol{P}_0$ of lengths $64, 128, 256, ..., 4096$ with minimized ℓ_2-norm. The used algorithm and the obtained sequences are available online [32].

The CCSK modulation maps an element c_k of the codeword $\boldsymbol{C}$ to the sequence $\boldsymbol{P}_{c_k}$ defined as the circular right shift of $\boldsymbol{P}_0$ by c_k positions

$$\boldsymbol{P}_{c_k} = \{P_0(i - c_k \bmod q)\}_{i=0,1,\ldots,q-1}. \tag{3}$$

Hence, the CCSK frame $\boldsymbol{F}$ is defined as the concatenation of N CCSK symbols

$$\boldsymbol{F} = [\boldsymbol{P}_{c_0}, \boldsymbol{P}_{c_1}, \ldots, \boldsymbol{P}_{c_{N-1}}]. \tag{4}$$

The CCSK modulation rate can be defined as $R_m = \frac{p}{q}$, and

the overall effective coding rate R_{eff} is given by $R_{eff} = R_c \times R_m = \frac{K}{N} \times \frac{p}{q}$. Since BPSK modulation is used, the effective spectral efficiency S_e is R_{eff} bits per channel use.

Before transmission, the generated frame $\boldsymbol{F}$ is composed of $N \times q$ BPSK symbols, and is then shaped by a half-raised cosine filter with a roll-off factor of 0.35 in our simulations. To summarize, generating the proposed coded frame at the transmitter side requires only simple operations (the GF encoder requires only XOR operations), which is particularly suitable to very low-cost IoT sensors.

B. Channel model

In this paper, we consider a low-cost sensor that sporadically transmits/receives small messages in an unslotted asynchronous ALOHA protocol, i.e., without prior knowledge of the time of arrival and the potential carrier frequency offset of the signal.

Let T_c and $T = q \times T_c$ (in seconds) be the duration of a chip and a CCSK symbol respectively. The receiver will over-sample the incoming signal with $\mathcal{O}$ samples per chip. In other words, the clock frequency F_e of the receiver Analog to Digital Converter (ADC) is equal to $F_e = \mathcal{O}/T_c$, with $\mathcal{O}$ the over-sampling factor (typically between 4 and 8). A half raised cosine filter is also applied at the receiver side. The frequency offset is assumed to be small enough to guaranty no interference between chips. By indexing the time by duration T_c of a chip (i.e. $\mathcal{O}$ clock cycles), it is possible to determine the time of arrival t_a as a real $x_a = t_a/T_c$ and by decomposing x_a as

$$x_a = n_a + r_a/\mathcal{O} + \epsilon_a, \tag{5}$$

where $n_a = \lfloor x_a \rfloor$, the integer part of x_a representing the time in number of chips, r_a the closest index of the clock cycle within a chip ($r_a \in \{0, 1, \ldots, \mathcal{O}-1\}$) and ϵ_a is the residual timing synchronization error, with $\epsilon_a \in [-\frac{1}{2\mathcal{O}}, \frac{1}{2\mathcal{O}}]$.

In the sequel, we consider that the oversampling factor is high enough so that ϵ_a is negligible and can be considered equal to 0. Moreover, we also assume that, by testing in parallel all the $\mathcal{O}$ hypothesis of the r_a values, we can always manage to set r_a equal to 0.

Carrier frequency errors are also considered, leading to a frequency offset F_o Hz affecting the received frame. In T_c seconds, the frequency offset generates a rotation $\frac{T_c F_o}{2\pi}$ radians between two consecutive chips. In the sequel, a normalized frequency offset $F = F_o T_c$ is used. The impact of F is to generate a rotation $\omega = 2\pi F q$ radians between two chips separated by a symbol duration. Finally, the initial phase offset φ is unknown too, where $\varphi \in [0,\ 2\pi]$. It is also assumed that there is enough time between each message to ensure no interference. In summary, the frame is received at chip index n_a can be defined as:

$$\begin{aligned} y(n) &= e^{j(n\frac{\omega}{q}+\varphi)}\boldsymbol{F}(n-n_a) + z(n), \text{if } n \in [n_a, n_a+Nq-1] \\ &= z(n), \text{ otherwise.} \end{aligned} \tag{6}$$

Without any prior information, ω and φ are supposed to be uniformly distributed in their respective interval ranges. The $z(n)$ realisations of a complex AWGN $\mathcal{CN}(0, \sigma^2)$, with zero mean and standard deviation $\sigma = \sqrt{10^{-\mathrm{SNR}/10}}$.

C. Time and Frequency decomposition

The blind detection algorithm splits the time and frequency domains into a regular grid composed of bins. Each bin is defined by a time span of ℓ chips, and a frequency span of size F_b (with a rotation $\omega_b = 2\pi F_b q$). We assume the normalized frequency offset F varies between $-F_{\max}$ and $F_{\max}$, so the number of frequency bins is equal to $N_F = \frac{2F_{\max}}{F_b}$. Thus, each bin corresponds to an arrival hypothesis of the frame with a coarse time and frequency precision. The detection method (illustrated hereafter in section III) is used in each bin to assess (hypothesis H1) or not (hypothesis H0) the arrival of a frame within the bin.

Every ℓ chips ($\ell \leq q$ typically), the last $N \times q$ received chips are extracted to form the vector $\boldsymbol{Y}_n = (y(n+i))_{i=0,1,\ldots,N\times q-1}$ (with $n = \gamma\ell$ is a time index). Then, at the entry of the β^{th} frequency detector, $\boldsymbol{Y}_{n,\beta} = \boldsymbol{Y}_n \odot \boldsymbol{E}_\beta$ is computed, where $\odot$ is the element-wise (or Hadamard) product of two vectors and $\boldsymbol{E}_\beta = (e^{-j\beta\omega_b i/q})_{i=0,1,\ldots,N\times q-1}$ is computed in order to compensate the frequency offset before entering the detector. Let us consider a frame arriving at chip index n_a with a normalized frequency offset F as in (6). By decomposing n_a as $n_a = \gamma_a\ell + \Delta$ and F as $F = \beta_a F_b + f_o$, we obtain $-\ell/2 < \Delta \leq \ell/2$ and the residual frequency f_o verifies $-F_b/2 < f_o \leq F_b/2$. We can deduce that the frame is optimally detectable in the bin (γ_a, β_a) since in this bin, the time and frequency offsets errors are minimized.

To lessen the notations, the frame $\boldsymbol{Y}_n$ processed at bin (γ_a, β_a) is denoted at chip level as the following

$$y(n) = e^{j(n\frac{\omega_o}{q}+\varphi)}\boldsymbol{F}(n-\Delta) + z(n), \tag{7}$$

where $\omega_o = 2\pi f_o q$ and $z(n)$ are independent realizations of a complex Gaussian noise $\mathcal{CN}(0, \sigma^2)$ of zero mean and variance σ^2, $\varphi \in [0, 2\pi]$, with $\Delta \in \{-\ell/2, \ldots, \ell/2\}$ and $\omega_0 \in [-\omega_b/2, \omega_b/2]$.

In the case of the reception of a frame in the optimal bin (hypothesis H1), the base band transmission model is thus a function of the following parameters: the time offset Δ, the residual rotation ω_o corresponding to residual frequency offset f_o, the initial phase offset φ, and the standard deviation σ of the complex AWGN. In the case of no reception (Hypothesis H0), the base band transmission model is

$$y(n) = z(n). \tag{8}$$

D. Demodulation of a QCSP frame

From the CCSK and NB-Code association, the de-mapping (i.e., demodulation) process is described in [21]. The input of a NB decoder can be given as the vector of log-likelihood values $\boldsymbol{L}_n = \{L_n(s) \triangleq \log(\mathcal{P}(\boldsymbol{P}_s|\boldsymbol{y}_n))\}_{s=0,1,\ldots,q-1}$, where $\boldsymbol{y}_n$ is a received block message of length q which starts at time n, i.e. $\boldsymbol{y}_n = (y(n), y(n+1), \ldots, y(n+q-1))$, assumed to be perfectly synchronized by the correct estimation of the offset parameters in (7), and $\mathcal{P}(\boldsymbol{P}_s|\boldsymbol{y}_n)$ is the probability that the transmitted sequence is $\boldsymbol{P}_s$ given that the received block message is $\boldsymbol{y}_n$. For a given element $s \in \mathrm{GF}(q)$, $L_n(s)$ can be expressed as the correlation between the received block

message $\boldsymbol{y}_n$ and expected message $\boldsymbol{P}_s$, $L_n(s) \cong \langle \boldsymbol{y}_n, \boldsymbol{P}_s \rangle$

$$\begin{aligned} L_n(s) &\cong \text{Real}\left(\sum_{i=0}^{q-1} y_n(i) P_s^*(i)\right) \\ &= \text{Real}\left(\sum_{i=0}^{q-1} y_n(i) P_0^*(i - s \bmod q)\right), \end{aligned} \tag{9}$$

for $s = 0, \ldots, q-1$, where $P_s^*(i)$ is the conjugate of $P_s(i)$ [1]. Hence, the log-likelihood vector $\boldsymbol{L}_n$ is the circular correlation between the received block message $\boldsymbol{y}_n$ of length q and the spreading sequence $\boldsymbol{P}_0$. It can be efficiently computed in the frequency domain as

$$\boldsymbol{L}_n = \text{IFFT}(\text{FFT}(\boldsymbol{y}_n) \odot \text{FFT}^*(\boldsymbol{P}_0)). \tag{10}$$

In order to feed the decoder with positive LLR values only, the vector $\boldsymbol{L}_n$ can be normalized with respect to the maximum value it contains as $\tilde{\boldsymbol{L}}_n = \max(\boldsymbol{L}_n) - \boldsymbol{L}_n$ [33]. This vector, measuring the reliability of the different possible sequences, is then fed directly to the NB-decoder to perform the decoding process, expected to correct errors encountered during transmission.

E. Detection problem

The detection problem investigated in the paper is how to determine which hypothesis is realized, based on the observation of the vector $\boldsymbol{Y}_n$ received at time n.

The problem consists in developing a reliable score function (or match filter) $S(\boldsymbol{Y}_n)$, that takes high values when H1 is fulfilled, and low values when H0 is true. Then, $S(\boldsymbol{Y}_n)$ is compared to a threshold U_0 in order to decide whether a new frame is present (H1) or not (H0). Let us recall some basic notions in detection theory that will be helpful for the rest of the article. In detection theory, the detector can produce one of four different cases:

- Miss detection: takes an erroneous decision by signaling the absence of any frame whereas a frame does exist, its probability $\mathcal{P}_{\text{md}} = \mathcal{P}(S(\boldsymbol{Y}_n) < U_0 |\ \text{H1})$.
- Correct detection: $\mathcal{P}(S(\boldsymbol{Y}_n) \geq U_0 |\ \text{H1})$, correctly detects an existing frame (the probability of correct detection is equal to $1 - \mathcal{P}_{\text{md}}$).
- False alarm: $\mathcal{P}_{\text{fa}} = \mathcal{P}(S(\boldsymbol{Y}_n) \geq U_0 |\ \text{H0})$, takes an erroneous decision by signaling the existence of a frame whereas a frame does not exist.
- Correct Absence: $\mathcal{P}(S(\boldsymbol{Y}_n) < U_0 |\ \text{H0})$, correctly indicates the absence of a frame (the probability of correct absence is equal to $1 - \mathcal{P}_{\text{fa}}$).

Note that when only part of a frame is inside the detector filter, the output $S(\boldsymbol{Y}_n)$ may become greater than U_0, potentially triggering early or late detection. Since $S(\boldsymbol{Y}_n)$ is maximized under hypothesis H1, it is natural to consider only this hypothesis in the detection investigation. Note that once a frame is detected, the synchronization process (not considered in the paper) should estimate the real time of arrival of the frame.

[1] In case of a BPSK modulation, there is no difference, but a CCSK modulation can also be considered using a CAZAC sequence where complex values exist.

III. Detection Method: Description of the Score Function

This section discusses in detail the proposed score function $S(\boldsymbol{Y}_n)$, which constitutes the core of the detection algorithm used to detect the CCSK frame. From the received data stream, a window $\boldsymbol{Y}_n$, of $N \times q$ chips, is extracted at time index n, and splitted into N consecutive blocks $\boldsymbol{y}_{n+kq}$, $k = 0, 1, ..., N-1$ each of q chips, i.e. $\boldsymbol{Y}_n = \{\boldsymbol{y}_{n+kq}\}_{k=0,1,\ldots,N-1}$. Using FFT operations, cross-correlation is performed between the N blocks $\{\boldsymbol{y}_{n+kq}\}_{k=0,1,\ldots,N-1}$ and the reference sequence $\boldsymbol{P}_0$ (10). Without loss of generality, let $\Delta \in [0, q/2]$, be the time shift (in number of chips) between the effective frame time of arrival and the one considered by the receiver. Note that a symmetrical effect exists when $\Delta \in [-q/2, 0]$.

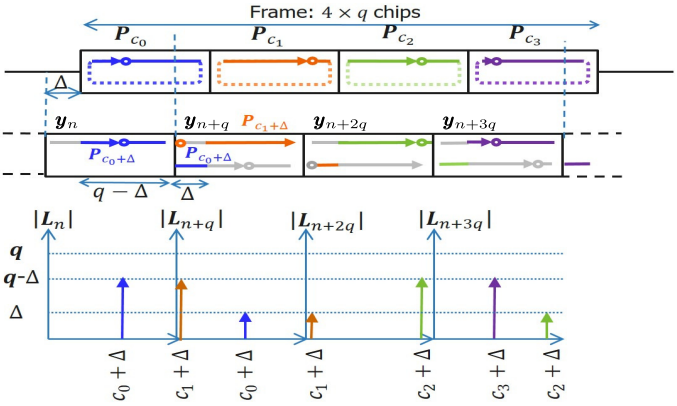

Fig. 2: Illustration of the frame detection principle for $N = 4$ symbols.

The best way to discuss and describe the proposed method (score function) is by giving an example. We assume that a frame contains $N = 4$ symbols as in Fig. 2, each of length q, the symbols (c_0, c_1, c_2, c_3) are associated with the four CCSK sequences $(\boldsymbol{P}_{c_0}, \boldsymbol{P}_{c_1}, \boldsymbol{P}_{c_2}, \boldsymbol{P}_{c_3})$, and a distinct color is associated to each symbol. In vector $\boldsymbol{y}_n$, there are $q - \Delta$ chips that are aligned with the first symbol of the received message of the frame, i.e. $\boldsymbol{P}_{c_0}$, or the $\boldsymbol{P}_0$ sequence circularly shifted by c_0 chips. Relatively to $\boldsymbol{y}_n$ and because of the delay Δ, the first Δ chips are null; then, the sequence starts at time $c_0 + \Delta \pmod q$ which is presented at the receiver side as the structure of another sequence $\boldsymbol{P}_{c_0+\Delta}$. Hence, $q - \Delta$ are aligned with the CCSK sequence $\boldsymbol{P}_{c_0+\Delta}$. Thus, the first correlation vector $\boldsymbol{L}_n$ related to vector $\boldsymbol{y}_n$ (i.e., $k = 0$), has a spike of height $q - \Delta$ at index $c_0 + \Delta \pmod q$. Thus, in the absence of noise, the maximum cross correlation vector magnitude $\max(|\boldsymbol{L}_n|)$ is equal to $q - \Delta$. Similarly, for the vector $\boldsymbol{y}_{n+q}$, there are Δ chips that are aligned with the first symbol $\boldsymbol{P}_{c_0}$ with an offset of $c_0 + \Delta$ chips (the sequence $\boldsymbol{P}_{c_0+\Delta}$). Thus, corresponding to Δ chips of the sequence $\boldsymbol{P}_{c_0+\Delta}$, the correlation vector $\boldsymbol{L}_{n+q}$ has a spike of magnitude Δ at index $c_0 + \Delta \pmod q$. Moreover, $\boldsymbol{y}_{n+q}$ contains $q - \Delta$ chips aligned with the second symbol $\boldsymbol{P}_{c_1+\Delta}$ of the transmitted message, which gives a spike of height $q - \Delta$ for $\boldsymbol{L}_{n+q}$ in position $c_1 + \Delta \pmod q$ (which is the correlation with the sequence $\boldsymbol{P}_{c_1+\Delta}$ and so on).

Hence, the received block $\boldsymbol{y}_{n+kq}$ has $q-\Delta$ chips of correlation with the CCSK sequence $\boldsymbol{P}_{c_k+\Delta}$ and Δ chips with the other sequence $\boldsymbol{P}_{c_{k-1}+\Delta}$. The first received symbol $\boldsymbol{y}_n$ is a special case as it has $q-\Delta$ correlation with the CCSK sequence $\boldsymbol{P}_{c_0+\Delta}$.

Thus, the score function can be obtained using a detection filter $S(\boldsymbol{Y}_n)$ of length N acting as a moving average filter

$$S(\boldsymbol{Y}_n) = \sum_{k=0}^{N-1} \max(|\boldsymbol{L}_{n+kq}|). \tag{11}$$

In the absence of noise with optimized $\boldsymbol{P}_0$ auto-correlation properties where $\langle \boldsymbol{P}_s, \boldsymbol{P}_{s'} \rangle \ll q$ for $s \neq s'$, the filter output gives $S(\boldsymbol{Y}_n) = N \times (q-\Delta)$. [2]

In the presence of AWGN noise, the detector compare $S(\boldsymbol{Y}_n)$ to a threshold U_0 to assess the arrival, or not, of a frame. The following section evaluates the detection performance of the QCSP frame in an asynchronous AWGN channel.

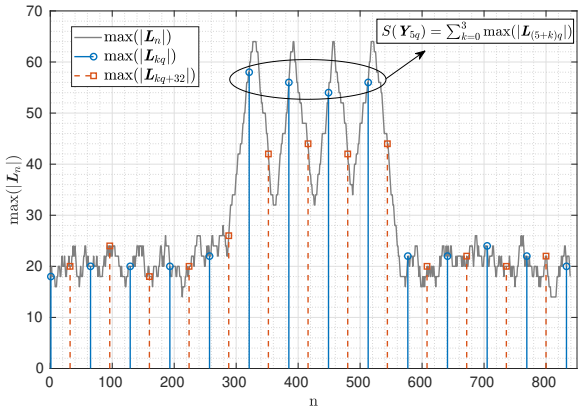

Fig. 3: Example of the score function calculation for a CCSK frame of size $N=4$, $q=64$ starting at time $n_a = 327 = 5q+\Delta$, where $\Delta = 7$. Random bits are assumed to be transmitted before and after the CCSK frame.

Fig. 3 gives an example of the calculation of $\boldsymbol{L}_n$ for a frame $\boldsymbol{Y}$ composed first of 326 random bits, then a QCSP frame of length $N=4$, $q=64$ starting at chip index $n_a = 327$ and finally, an additional 320 random bits. The continuous gray curve is the output of the maximum of the correlation vectors $\max(|\boldsymbol{L}_n|)$ at each chip index n. In this example, the time bin size is defined as $\ell = q/2 = 32$, i.e., only $\max(|\boldsymbol{L}_{64k}|)$, and $\max(|\boldsymbol{L}_{64k+32}|)$, $k \in \mathbb{N}$, are effectively computed using (10). The values used to compute the score function $S(\boldsymbol{Y}_{n=5\times 64})$ which correspond to the minimum time offset error $\Delta = n_a -$ $(5q) = 7$ are also shown. It is worth noticing that the time sliding windows method proposed in [34] computes the score function $S_n(\mathbf{Y})$ for every value of n, thus giving an optimal time bin size $\ell = 1$. This method has a complexity in the order of $O(q)$ per chip. It is thus applicable for small values of q ($q \leq 128$, typically).

[2]In order to draw benefits from the second maximum shown in Fig. 2, it is possible to add two consecutive correlation vectors before taking its maximum (Sum of Correlation (SC) method). The score function becomes

$$S^{(\mathrm{SC})}(\boldsymbol{Y}_n) = \sum_{k=0}^{N-2} \max(|\boldsymbol{L}_{n+kq} + \boldsymbol{L}_{n+kq+1}|). \tag{12}$$

This method is not examined in the paper owing to space limitations, but it is worth mentioning that, compared to the score function $S(\boldsymbol{Y}_n)$, $S^{(\mathrm{SC})}(\boldsymbol{Y}_n)$ gives a slight improvement of detection capacity when Δ is close to $q/2$, and gives a few dB penalty when Δ is close to 0. It is also more sensitive to a frequency offset, since the duration of coherent integration is doubled.

IV. Theoretical Model

In this section, we derive the formal performance model of the frame detection algorithm discussed in the previous section. This model allows to avoid expensive performance estimation through MC simulation. It gives insights to analyze the impact of each parameter on the detection performance. In this section, variable n is omitted from expressions $\boldsymbol{L}_{n+kq}$ and $\boldsymbol{y}_{n+kq}$ to lighten the notations

A. Correlation Expressions

Let us first express the exact expression of $L_{kq}(s)$, see (9) for each value of s. Then, we derive the probability law of $|L_{kq}(s)|$ with and without signal.

Definitions and notations: Let us first consider the two vectors $\boldsymbol{g} = [g_0\ g_1\ \ldots\ g_{L-1}]$, and $\boldsymbol{h} = [h_0\ h_1\ \ldots\ h_{L-1}]$. Then, we define the following vector-operators that help the formulation of the theoretical model:

- Sectioning a vector from index a to b:

$$\boldsymbol{g}_a^b = [g_a\ g_{a+1}\ \ldots\ g_b].$$

- Concatenation of two vectors $\boldsymbol{g}$ and $\boldsymbol{h}$:

$$\boldsymbol{g} \coprod \boldsymbol{h} = [g_0\ \ldots\ g_{L-1}\ h_0\ \ldots\ h_{L-1}].$$

- Linear Right and Left shifts of vector $\boldsymbol{g}$ by Δ positions:

$$\mathcal{R}^{\Delta}(g) = \mathbf{0}_0^{\Delta-1} \coprod \boldsymbol{g}_0^{L-\Delta-1}$$
$$\mathcal{L}^{\Delta}(g) = \boldsymbol{g}_{\Delta}^{L-1} \coprod \mathbf{0}_0^{\Delta-1},$$

where $\mathbf{0}_0^{\Delta-1}$ is a zero vector of length Δ.

Based on the discussion in previous sections and Eq. (7), frame $\boldsymbol{Y} = \{\boldsymbol{y}_{kq}\}_{k=0,1,\ldots,N-1}$ at the optimal bin can be rewritten in vector-operational form as:

$$\boldsymbol{Y} = \mathrm{e}^{j\varphi} \left(\mathcal{R}^{\Delta}(\boldsymbol{F}) \odot \boldsymbol{\Phi} \right) + \boldsymbol{Z}, \tag{13}$$

where φ is the initial phase offset, $\mathcal{R}^{\Delta}(\boldsymbol{F})$ the delayed CCSK frame by Δ chips, and $\boldsymbol{\Phi} = \{\mathrm{e}^{j2\pi f_o n}\}_{0\leq n\leq Nq-1}$ a vector representing the effect of frequency offset f_o. $\boldsymbol{Z}$ is the complex AWGN vector: $\boldsymbol{Z} = \boldsymbol{Z}_I + j\boldsymbol{Z}_Q$, where $\boldsymbol{Z}_I$ and $\boldsymbol{Z}_Q$ follow complex Normal distribution $\mathcal{CN}(0, \sigma^2)$.

Due to the specific structure of the CCSK modulation (all the sequences are cyclically shifted versions of the reference sequence $\boldsymbol{P}_0$), the delayed Frame $\mathcal{R}^{\Delta}(\boldsymbol{F})$ in (13) can be expressed as:

$$\mathcal{R}^{\Delta}(\boldsymbol{F}) = \left(\mathbf{0}_0^{\Delta-1} \coprod (\boldsymbol{P}_{c_0})_0^{q-\Delta-1} \right) \coprod \left(\coprod_{k=1}^{N-1} \left((\boldsymbol{P}_{c_{k-1}})_{q-\Delta}^{q-1} \coprod (\boldsymbol{P}_{c_k})_0^{q-\Delta-1} \right) \right). \tag{14}$$

Finally, the first received vector $\boldsymbol{y}_0$ can be written as

$$\boldsymbol{y}_0 = \mathrm{e}^{j\varphi} \mathcal{R}^{\Delta}(\boldsymbol{P}_{c_0}) \odot \boldsymbol{\Phi}_0^{q-1} + \boldsymbol{Z}_0^{q-1}, \tag{15}$$

and $\boldsymbol{y}_{kq}$, $k>0$ as

$$\boldsymbol{y}_{kq} = \mathrm{e}^{j\varphi}\left\{\mathcal{L}^{q-\Delta}\left(\boldsymbol{P}_{c_{k-1}}\right)+\mathcal{R}^{\Delta}\left(\boldsymbol{P}_{c_k}\right)\right\}\odot\boldsymbol{\Phi}_{kq}^{kq+q-1}+\boldsymbol{Z}_{kq}^{kq+q-1}. \tag{16}$$

Exact expression of $L_{kq}(s)$: Taking into consideration the expression of $\boldsymbol{y}_{kq}$ defined in (16) and the linearity property of the scalar product, the correlation $L_{kq}(s)=\langle\boldsymbol{y}_{kq},\boldsymbol{P}_s\rangle$ can be expressed as

$$L_{kq}(s)=L_{kq}^{-}(s)+L_{kq}^{+}(s)+z_{kq}(s), \tag{17}$$

where

$$\begin{aligned}L_{kq}^{-}(s)&=e^{j\varphi}\langle\mathcal{L}^{q-\Delta}\left(\boldsymbol{P}_{c_{k-1}}\right)\odot\boldsymbol{\Phi}_{kq}^{kq+q-1},\boldsymbol{P}_s\rangle\\&=e^{j\psi_k}\sum_{n=0}^{\Delta-1}P(n-c_{k-1}-\Delta)P(n-s)\mathrm{e}^{j2\pi f_o n},\end{aligned} \tag{18}$$

$$L_{kq}^{+}(s)=e^{j\psi_k}\sum_{n=\Delta}^{q-1}P(n-c_k-\Delta)P(n-s)\mathrm{e}^{j2\pi f_o n}, \tag{19}$$

and

$$z_{kq}(s)=\langle\boldsymbol{Z}_{kq}^{kq+q-1},\boldsymbol{P}_s\rangle. \tag{20}$$

The phase offset $\psi_k=\varphi+kq2\pi f_o$ represents the sum of the initial phase shift φ and the contribution of the residual frequency offset f_o on the k^{th} received block Y_{kq}.

Let us analyze (17), (18) and (19) in particular useful cases.
a) When $k=0$, (17) will be reduced to $L_0(s)=L_0^{+}(s)+z_0(s)$.
b) When $s=c_{k-1}+\Delta$, (18) gives

$$L_{kq}^{-}(c_{k-1}+\Delta)=e^{j\psi_k}\sum_{n=0}^{\Delta-1}e^{j2\pi f_o n}=e^{j\psi_k^{-}}\left(\frac{\sin\left(\pi f_o\Delta\right)}{\sin\left(\pi f_o\right)}\right), \tag{21}$$

where $\psi_k^{-}=\psi_k+\pi f_o(\Delta-1)$.
c) When $s=c_k+\Delta$, (19) gives

$$L_{kq}^{+}(c_k+\Delta)=e^{j\psi_k^{+}}\left(\frac{\sin\left(\pi f_o(q-\Delta)\right)}{\sin\left(\pi f_o\right)}\right), \tag{22}$$

where $\psi_k^{+}=\psi_k+\pi f_o(q+\Delta-1)$.
d) In the particular case where $c_{k-1}=c_k=c$, when $s=c+\Delta$:

$$L_{kq}(c+\Delta)=e^{j(\psi_k+\pi f_o(q-1))}\left(\frac{\sin(\pi f_o q)}{\sin(\pi f_o)}\right)+z_{kq}(s). \tag{23}$$

e) It is worth adding that when there is no phase and frequency offsets ($\varphi=0$ and $f_o=0$), then (21) and (22) give $L_{kq}^{-}(c_{k-1}+\Delta)=\Delta$ and $L_{kq}^{+}(c_k+\Delta)=(q-\Delta)$ respectively, as shown in Fig. 2. From the formal expression of $L_{kq}(s)$ for any value of s, it is possible to derive the exact probability law of $\max\left(|\boldsymbol{L}_{kq}|\right)$ used to compute $S(\boldsymbol{y})$ in (11). Finally, according to (20), $z_{kq}(s)$ is the sum of q independent Complex Gaussian Random Variables (CGRV) $\mathcal{CN}(0,\sigma^2)$ multiplied by +1 or by -1. Thus, $z_{kq}(s)$ is a realization of Complex Gaussian distribution of law $\mathcal{CN}(0,q\sigma^2)$.

Probability law of $L_{kq}(s)$: Under the hypothesis H0 (no signal), the terms L_{kq}^{-} and L_{kq}^{+} of (17) are null and thus, for each s, $L_{kq}(s)=z_{kq}(s)$ is a CGRV of law $\mathcal{CN}(0,q\sigma^2)$ as defined before.

Under the hypothesis H1 (signal exists), when $k>0$, $L_{kq}(s)=L_{kq}^{-}(s)+L_{kq}^{+}(s)+z_{kq}(s)$. The first two terms are deterministic. Their sum can be expressed in polar coordinates as $L_{kq}^{-}(s)+L_{kq}^{+}(s)=\rho_k(s)e^{j\theta_k(s)}$, and thus $L_{kq}(s)$ is a CGRV of law $\mathcal{CN}(\rho_k(s)e^{j\theta_k(s)},q\sigma^2)$. Since we are interested in the absolute value of $L_{kq}(s)$, the phase $\theta_k(s)$ has no impact. The value of $\rho_k(s)=|L_{kq}^{-}(s)+L_{kq}^{+}(s)|$ takes particular values for $s=c_{k-1}+\Delta$ and $s=c_k+\Delta$, as shown in (21) and (22). For the first symbol, when $k=0$, $L_0(s)=L_0^{+}(s)+z_0(s)$, and thus $\rho_0(s)=|L_0^{+}(s)|$.

In next subsections, the distributions of the absolute values $|L_{kq}(s)|$, $s=0,1,\ldots,q-1$ are derived.

B. Probability distributions of $|\boldsymbol{L}_{kq}(s)|$ and maximum of $|\boldsymbol{L}_{kq}(s)|$

In this section we discuss the Probability Density Function (PDF) as well as the Cumulative Distribution Function (CDF) of $|L_{kq}(s)|$ the absolute value of each of the CGRVs representing the elements of the correlation vector $L_{kq}(s)$, $s=0,1,\ldots,q-1$, defined in previous section. Then we derive the PDF of the maximum value of $|L_{kq}(s)|$ in both hypothesis H0 and H1.

PDF and CDF of the absolute value of $L_{kq}(s)$, $|L_{kq}(s)|$: The dependency of $|L_k(s)|$ on the index $k>0$ depends only on the couple values (c_{k-1},c_k). It is thus convenient to replace (c_{k-1},c_k) by (a,b) to lighten notation. With this notation, $L_{(a,b)}(s)$ is a CGRV of law $\mathcal{CN}(\rho_{(a,b)}(s)e^{j\theta_{(a,b)}(s)},q\sigma^2)$, where $\rho_{(a,b)}(s)$ and $\theta_{(a,b)}(s)$ are the module and the phase of $L_{(a,b)}^{-}(s)+L_{(a,b)}^{+}(s)$, respectively. Thus, $|L_{(a,b)}(s)|$ is a Rician distribution with the following PDF and CDF [35]:

$$\begin{aligned}f_{|L_{(a,b)}(s)|}(x)&=\frac{2x}{q\sigma^2}\mathrm{e}^{\left(-\frac{x^2+\rho_{(a,b)}(s)^2}{q\sigma^2}\right)}I_0\left(\frac{2x\rho_{(a,b)}(s)}{q\sigma^2}\right),\\F_{|L_{(a,b)}(s)|}(x)&=1-Q_1\left(\frac{\rho_{(a,b)}(s)}{\sigma\sqrt{q/2}},\frac{x}{\sigma\sqrt{q/2}}\right),\end{aligned} \tag{24}$$

where $x\in[0,+\infty[$, $I_0(z)$ is the modified Bessel function of the first kind with order zero and Q_1 is the Marcum Q-function. For a given couple $a=c_{k-1}$ and $b=c_k$, $F_{|L_{(a,b)}(s)|}(x)$ is plotted in Fig 4 for $s=c_{k-1}+\Delta$, $s=c_k+\Delta$ and the other $q-2$ cases when $s\neq c_{k-1}+\Delta$, $s\neq c_k+\Delta$.

PDF and CDF of the Maximum value of $|L_{kq}(s)|$ for H1: Let us define the first hypothesis of our proposed theoretical model. According to (20), for any couple (s,s'), we have the inter-correlation $\mathbb{E}[z_{kq}(s),z_{kq}(s')]$ between $z_{kq}(s)$ and $z_{kq}(s')$ equal to $\langle\boldsymbol{P}_s,\boldsymbol{P}_{s'}\rangle$. Since $z_{kq}(s)$ and $z_{kq}(s')$ are both Gaussian variables of zero mean, they are independent if, and only if, $\mathbb{E}[z_{kq}(s),z_{kq}(s')]=0$. This hypothesis will be assumed in the rest of the paper since the sequence $\boldsymbol{P}_0$ is carefully selected so that $s\neq s'\Rightarrow\langle\boldsymbol{P}_s,\boldsymbol{P}_{s'}\rangle\ll q$. In others words, variables $z_{kq}(s)$ will be considered independent from each other.

Let us first consider $k>0$ and define $M_{(a,b)}$ as the maximum of the absolute values of $L_{(a,b)}(s)$, i.e. $M_{(a,b)}=\max\{|L_{(a,b)}(s)|,s\in GF(q)\}$. The independence hypothesis

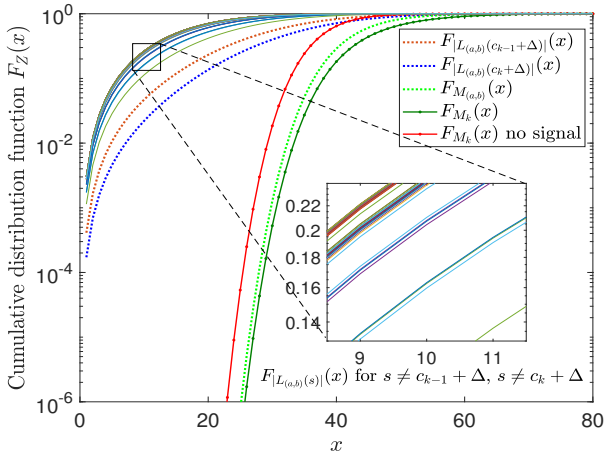

Fig. 4: Illustration of different CDF equations for a given GF(64) received block $\boldsymbol{y}_{kq}$ at $E_s/N_0 = -7$ dB, $\Delta = 24$ chips and $\omega_o = \pi/4$.

of the $z_{(a,b)}(s)$ variables also implies the independence of the $|z_{(a,b)}(s)|$ variables. Thus, the CDF of the $M_{(a,b)}$ denoted by $F_{M_{(a,b)}}$ is defined as the product of the elementary CDFs of each element $F_{|L_{(a,b)}(s)|}$, $s = 0, 1, ..., q-1$

$$F_{M_{(a,b)}}(x) = \prod_{s=0}^{q-1} F_{|L_{(a,b)}(s)|}(x), \tag{25}$$

for $x \in [0, +\infty[$. All the CDF functions implied in (25) are plotted in Fig. 4 for a given couple $a = c_{k-1}$ and $b = c_k$. Since all the couples (a, b) are equally likely, the average value of $F_{M_k}(x)$ is given by marginalizing $F_{M_{(a,b)}}(x)$ over all possible couples, i.e.,

$$F_{M_k}(x) = \frac{1}{q^2} \sum_{(a,b)} F_{M_{(a,b)}}(x), \tag{26}$$

as shown in Fig 4.

When $k = 0$, M_0 depends only on c_0 and we can replace the index 0 by the value (b) to be consistent with the previous notation, i.e., $M_0 = M_{(b)}$. Thus

$$F_{M_0}(x) = \frac{1}{q} \sum_{(b)} \prod_{s=0}^{q-1} F_{|L_{(b)}(s)|}(x). \tag{27}$$

The PDF of the maximum value of the absolute correlation vector denoted by f_{M_k} can be obtained by taking the derivative of F_{M_k}.

$$f_{M_k}(x) = \frac{dF_{M_k}(x)}{dx}. \tag{28}$$

The detection filter described in (11) takes the sum of N maximum values over a window of N blocks Y_{kq}. Thus the score function can be expressed as

$$S = \sum_{k=0}^{N-1} M_k. \tag{29}$$

In the sequel, we will assume that the M_k, $k = 0, 1, \ldots, N-1$, are independent and identically distributed random variables with common probability density function f_{M_k}. This is an approximation because two consecutive values $|L_{kq}(s)|$ and $|L_{k+1}(s)|$ are not necessarily uncorrelated since the same c_k value is used in both of them. Nevertheless, considering the set of couples L_{2k}, $k = 1..N/2$, they are thoroughly random as well as for the set $L_{2K+1}, k = 0, ..., N/2 - 1$. If N is large enough, the space is explored almost randomly. Thus, the PDF of the random variable S can be defined as the convolution of f_{M_k}, $k = 0, 1, \ldots, N-1$:

$$\begin{aligned} f_S(x) &= f_{M_0}(x) * f_{M_1}(x) * \cdots * f_{M_{N-1}}(x) \\ &= f_{M_0}(x) * f_{M_k}^{*(N-1)}(x), \end{aligned} \tag{30}$$

where $f_{M_k}^{*(N-1)}(x)$ is the $(N-1)$-fold convolution power of $f_{M_k}(x)$ and $x \in [0, +\infty[$. It is worth mentioning that as the number of symbols N in a packet increases, f_S converges to a normal distribution according to the central limit theorem. Under the hypothesis H1, $f_S(x)$ will be denoted as $f_S^{\mathrm{H1}}(x)$.

CDF and PDF of the Maximum value of $|L_{kq}(s)|$ for H0: The distribution of $L_{kq}(s)$ when no frame has been transmitted was given as complex GRV $\mathcal{CN}(0, q\sigma^2)$. In this case, the absolute value of the complex number $L_{kq}(s)$ is a random variable following the Rayleigh distribution [35], where the CDF and PDF of $|L_{kq}(s)|$ are given in (31) for $x \in [0, +\infty[$:

$$\begin{aligned} F_{|L_{kq}(s)|}(x) &= 1 - \mathrm{e}^{\left(-\frac{x^2}{q\sigma^2}\right)}, \\ f_{|L_{kq}(s)|}(x) &= \frac{2x}{q\sigma^2} \mathrm{e}^{\left(-\frac{x^2}{q\sigma^2}\right)}. \end{aligned} \tag{31}$$

Note that (31) is just a particular case of (24) when $\rho = 0$. The analysis done in section IV-B can be applied again. The PDF of the maximum value of $|L_{kq}(s)|$ can be obtained by calculating first its CDF,

$$F_{M_k}(x) = \prod_{s=0}^{q-1} F_{|L_{kq}(s)|}(x) = \left[1 - \mathrm{e}^{\left(-\frac{x^2}{q\sigma^2}\right)}\right]^q, \tag{32}$$

for $x \in [0, +\infty[$, that is also illustrated in Fig 4, and then finding its derivative $f_{M_k}(x)$ such that,

$$f_{M_k}(x) = \frac{2x}{\sigma^2} \mathrm{e}^{\left(-\frac{x^2}{q\sigma^2}\right)} \left[1 - \mathrm{e}^{\left(-\frac{x^2}{q\sigma^2}\right)}\right]^{q-1}. \tag{33}$$

Finally, under hypothesis H0 the PDF of the random variable S, sum of M_k, can be defined as the convolution of f_{M_k}, $k = 0, 1, \ldots, N-1$:

$$f_S^{\mathrm{H0}}(x) = f_{M_k}^{*N}(x), \tag{34}$$

which is the N-fold convolution power of $f_{M_k}(x)$.

C. Empirical Verification of the Theoretical Model by MC Simulation

In the previous section we derived the PDFs $f_S^{\mathrm{H1}}(x) \backsim \mathcal{P}(X = S(y)|\ \mathrm{H1})$ in (30) and $f_S^{\mathrm{H0}}(x) \backsim \mathcal{P}(X = S(y)|\ \mathrm{H0})$ in (34) over AWGN channel when the CCSK frame exists or is absent, respectively.

In order to check the validity of the hypothesis taken to build the theoretical model, we compare it with the MC simulation,

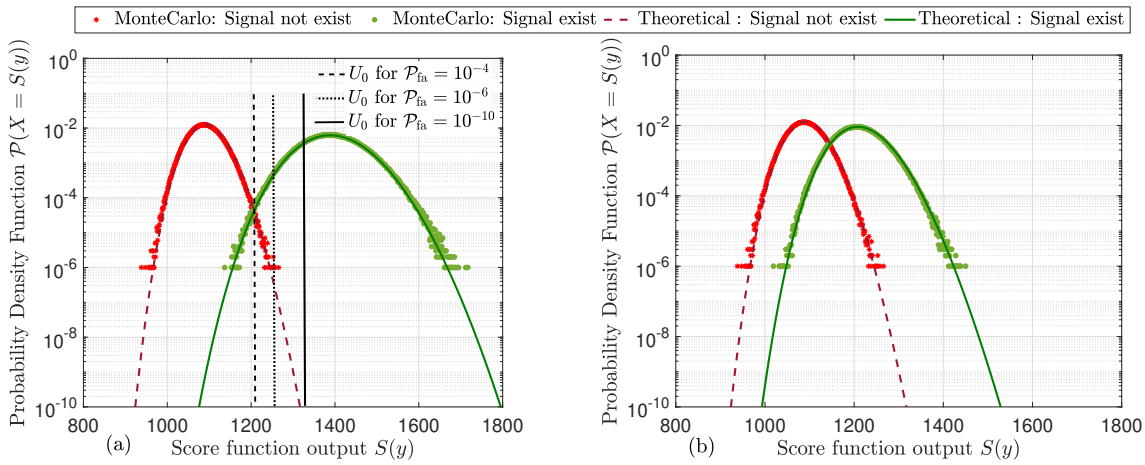

Fig. 5: MC and Theoretical PDFs in both hypothesis H0 and H1, for a CCSK frame of $N = 20$ symbols in GF(64) for the first scenario **(a)** $E_s/N_0 = -10$ dB, $\Delta = 0$, no frequency offset and for the second scenario **(b)** $E_s/N_0 = -10$ dB, $\Delta = 16$, $\omega_o = \pi/2$.

when 10^6 CCSK frames are transmitted, in case of a frame length $N = 20$ GF(64) symbols over complex AWGN channel of E_s/N_0 = -10 dB. Two different scenarios are tested, the first one (see Fig 5.a) assesses perfect synchronization conditions ($\Delta = 0, w_o = 0$), and the second case (see Fig 5.b) is considered for $\Delta = q/4$ and $w_o = \pi/2$. As we can see in both cases, the probability distribution functions in the theoretical model fit exactly the MC simulations. It is worth noting that in the theoretical model, we can go through very low values in probabilities (here 10^{-10}) without the need to run 10^{10} iterations of a MC simulation for transmitting 10^{10} CCSK frames for example. Thus, the detection performance can be found through the derived theoretical model without the need to conduct extensive MC simulations.

Effect of the threshold value U_0***:***

Fig. 5 (a) also illustrates three different threshold values that correspond to various probabilities of false alarm $\mathcal{P}_{\text{fa}} = 10^{-4}, 10^{-6}$ and 10^{-10} vs. the output of the correlation filter over a Gaussian channel. It can be clearly inferred from Fig. 5 (a) that the threshold value U_0 allows a trade-off between $\mathcal{P}_{\text{fa}}$ and $\mathcal{P}_{\text{md}}$. In fact, in a perfect detector, both probabilities should be equal to zero to determine perfectly the presence or not of a new frame. In practice, a high value of U_0 decreases $\mathcal{P}_{\text{fa}}$ but increases $\mathcal{P}_{\text{md}}$, whereas a low value of U_0 has the symmetrical effect. For example, at threshold value $U_0 = 1250$ that corresponds to $\mathcal{P}_{\text{fa}} = 10^{-4}$, the probability of miss detection is approximately $\mathcal{P}_{\text{md}} = 10^{-4}$. This value increases to $\mathcal{P}_{\text{md}} = 5 \times 10^{-3}$ for U_0 corresponding to $\mathcal{P}_{\text{fa}} = 10^{-10}$. The value of U_0 is selected depending on the system requirements; in the sequel, $\mathcal{P}_{\text{fa}}$ is set to 10^{-6}. This threshold value can be changed according to the required application. $\mathcal{P}_{\text{fa}}$ can be increased in a base station that can process false alarm at higher rate while in a sensor, it can be reduced (thus have higher miss detection rate) to avoid wasting energy while trying to decode false signal.

V. Results and Discussions

In this section, we first assess the detection performance of the system according to the following QCSP parameters: Galois field order q and number of CCSK symbols in a frame N based on the detection probabilities $\mathcal{P}_{\text{md}}$ and $\mathcal{P}_{\text{fa}}$ under low SNR (expressed as E_s/N_0) values. Next, we examine the effect of the time and frequency offsets on the system performance in an asynchronous channel. Subsequently, a Detection-Correction approach is analyzed based on the detection results obtained and the frame error-correction rates using the NB-LDPC decoder and the normal approximation equation that is used by Polyanskiy in [29] as the definition of the maximal achievable coding rate in the finite code-length regime. Finally, we set a comparison with up-to-date codes used for short packet transmission. All the up-coming results are obtained thanks to MC simulation that stopped after reaching 100 frames of errors. Also, all the results are confirmed by the theoretical performance model.

A. Performance Analysis: Effect of Galois Field Order $q = 2^p$

In this section, we study the effect of spreading sequence length q needed for CCSK modulation, i.e., or the order of Galois Field $q = 2^p$. For that, we fix the following set of parameters needed for generating a QCSP frame and vary the value of q for illustrating its effect on the detection performance:

- Number of CCSK symbols N: $N = 120$.
- Threshold value U_0: is determined for a $\mathcal{P}_{\text{fa}} = 10^{-6}$.
- Perfect time and frequency synchronization: $\Delta = 0$, $w_0 = 0$.

Fig. 6 shows the simulation results of $\mathcal{P}_{\text{md}}$ vs. E_s/N_0 for $q = 2^p$ ranging from $p = 6$ up to $p = 12$. For $q = 64$, $\mathcal{P}_{\text{md}}$ is plotted for three different values of $\mathcal{P}_{\text{fa}}$: 10^{-4}, 10^{-6} and 10^{-10}. As expected, $\mathcal{P}_{\text{md}}$ increases when $\mathcal{P}_{\text{fa}}$ decreases, i.e., when the threshold U_0 value increases. So the value of U_0

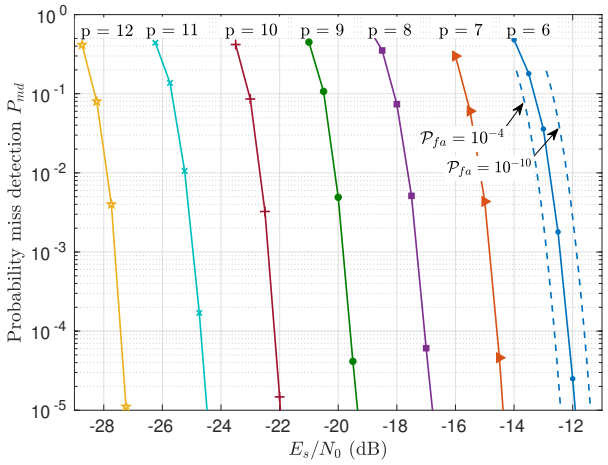

Fig. 6: $\mathcal{P}_{\text{md}}$ and $\mathcal{P}_{\text{fa}}$ as function of E_s/N_0 for a CCSK frame of $N = 120$ symbols for different orders $q = 2^p$, in an ideally synchronized channel.

in the system will be selected based on the desired trade-off $\mathcal{P}_{\text{fa}}$ vs $\mathcal{P}_{\text{md}}$ according to the application requirements. This observation is valid for $q > 64$, but the corresponding curves of $\mathcal{P}_{\text{md}}$ are omitted for the sake of figure simplicity. In our work, U_0 is selected in order to have $\mathcal{P}_{\text{fa}} = 10^{-6}$. As shown, the level of E_s/N_0 required to obtain an acceptable $\mathcal{P}_{\text{md}}$ of the order of 10^{-4} is -12.15 dB when $q = 64$, and decreases as q increases to go down to -27.55 dB when $q = 4096$.

B. Performance Analysis: Effect of the number of CCSK symbols N

This section examines the minimum number of symbols in the QCSP frame required for a reliable detection of a frame of finite length.

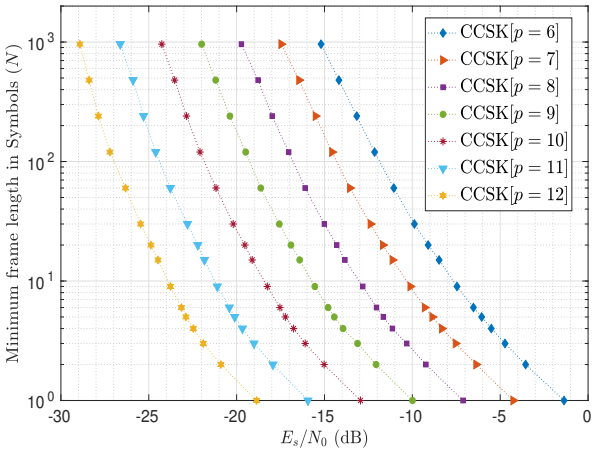

Fig. 7: Minimum number of CCSK symbols N in the QCSP frame, needed to guarantee $\mathcal{P}_{\text{md}} \leq 10^{-4}$ and $\mathcal{P}_{\text{fa}} \leq 10^{-6}$ at different E_s/N_0, for different CCSK order p in an ideally synchronized channel.

Fig. 7 shows the minimum number of CCSK frame symbols N needed to guarantee $\mathcal{P}_{\text{md}} = 10^{-4}$ and $\mathcal{P}_{\text{fa}} = 10^{-6}$, in an ideally synchronized channel (no frequency and no time offset), as function of E_s/N_0, for $p = 6$ (right-most curve) to $p = 12$ (left-most curve). Each point can also be seen as number of chips $N_q = N \times q$. According to the curves, at E_s/N_0 of -5 dB, at least 4, 2 and 1 CCSK symbols are required for the CCSK order of $p = 6$, $p = 7$ and $p \geq 8$ respectively, to obtain both $\mathcal{P}_{\text{md}} \leq 10^{-4}$ and $\mathcal{P}_{\text{fa}} \leq 10^{-6}$.

C. Performance Analysis: Effect of time and frequency offsets

The effect of both time and frequency shifts (see (7)) on the detector performance is discussed in this section. We consider the frame of length $N = 120$ symbols and of order $p = 6$. Fig. 8 plots the minimum E_s/N_0 needed, for predefined probabilities ($\mathcal{P}_{\text{fa}} = 10^{-6}$ and $\mathcal{P}_{\text{md}} = 10^{-4}$), as a function of temporal offset Δ for different values of frequency offsets ω_o. The figure is divided into two mirrored sides. The left hand side represents the result of the worst case scenario when the couple time and frequency offsets equal $|\Delta|$ and $|\omega_o|$ respectively, while the right hand side represents the result of the average case scenario when the couple time and frequency offsets are uniformly seen in $[-\Delta, \Delta]$ and $[-\omega_o, \omega_o]$ respectively, where $\omega_o = 0, \pi/4, \pi/2$ and π. The latter is a more accurate scenario since Δ and ω_o are uniformly distributed in their respective intervals.

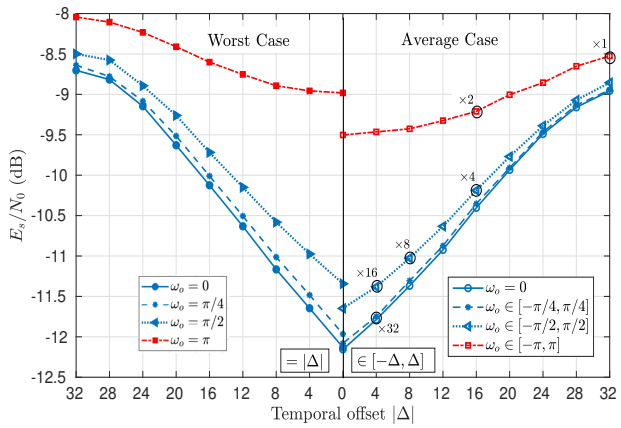

Fig. 8: Minimum E_s/N_0 required as function of different Δ and ω_0 values, for defined probabilities ($\mathcal{P}_{\text{fa}} = 10^{-6}$ and $\mathcal{P}_{\text{md}} = 10^{-4}$), in a CCSK frame of $N = 120$ and order $p = 6$.

A maximal temporal offset equals to $|\Delta| = 32$ corresponds to a temporal bin length $\ell = 64$. Similarly, a maximal frequency offset equals to $|\omega_0| = \pi$ corresponds to a frequency bin of size $\omega_b = 2\pi$. For this grid size, the required SNR is equal to -8.5 dB. The associated complexity of the decoder for a bin of size $(\omega_b, \ell) = (2\pi, 64)$ will be denoted by 1 (see circle noted $\times 1$ in Fig. 8). There are two possibilities to halve the bin size in order to get better detection performance. This can be achieved by halving the frequency dimension, i.e., using bins of size $(\omega_b, \ell) = (\pi, 64)$. In this case, the required SNR for detection is -8.8 dB. However, it is more efficient to halve the time dimension, i.e., using bins of size $(\omega_b, \ell) = (2\pi, 32)$. In the later case, the required SNR for detection is reduced down to -9.25 dB. This solution is indicated by the circle $\times 2$

(to reflect that the number of bins is doubled) in Fig. 8. By continuing recursively this process, the optimal solutions of complexities $\times 4$, $\times 8$, $\times 16$ and $\times 32$ are indicated in Fig. 8. The associated SNR are -10.2 dB, -11 dB, -11.4 dB and -11.8 dB, respectively. In the sequel, the $\times 32$ solution with bin size $(\omega_b, \ell) = (\pi/2, 8)$ will be considered.

D. Detection-Correction approach and a case-study example

After studying the detection performance of the QCSP system in the previous sections, we will first assess the error-correction performance and gives the upper bound limit that can be reached thanks to Polyanskiy's equation in [29]. Then we'll discuss the trade-off approach through a case-study example.

1) Polyanskiy's Bound and CCSK-NB-LDPC decoder: The maximum achievable coding rate, denoted by R_c^*, for error correction codes with error probability $\mathcal{P}_\epsilon$ (where $\mathcal{P}_c = 1 - \mathcal{P}_\epsilon$), can be tightly approximated, for $N \geq 100$, as in [29] by

$$R_c^* \approx R - \sqrt{\frac{V}{N}} Q^{-1}(\mathcal{P}_\epsilon), \tag{35}$$

where R is the channel capacity (maximum rate achievable in the asymptotic regime), V is the channel dispersion (defined in [29]) and Q^{-1} the inverse Q function where $Q(x) = \frac{1}{\sqrt{2\pi}} \int_x^\infty \exp\left(-\frac{u^2}{2}\right) du$. We use the above approximation (known as the *normal approximation*) as a definition of the maximum achievable coding rate in the finite code-length regime. In [29] the channel dispersion parameter is defined as

$$V = H_2(U|Y) - H(U|Y)^2, \tag{36}$$

where $H(U|Y)$ is the conditional entropy of the channel input U given the channel output Y, and

$$H_2(U|Y) \triangleq \mathbb{E}_Y \left[-\sum_{s \in \mathbb{Z}_q} L(s) (\log_q(L(s))^2 \right], \tag{37}$$

where $L(s) \triangleq \mathcal{P}(U = s|Y)$ denotes the conditional probability distribution of U given Y. Hence, $H_2(U|Y)$ can be conveniently estimated by MC simulation.

In the proposed QCSP system, we will study the NB-Code rates R_c for $R_c = 1/3, 1/2$ and $3/5$. So we can use (35) to find the corresponding minimum probability of error that can be reached at each E_s/N_0 and that is defined as:

$$\mathcal{P}_\epsilon^* = Q\left(-\frac{R_c - R}{\sqrt{V/N}} \right). \tag{38}$$

Let us consider a QCSP frame over GF(64), with frame of $N = 120$ symbols. So for $R_c = 1/3, 1/2$ and $3/5$ we have 40, 60 and 72 information GF(2^6) symbols respectively. We also assume a perfectly synchronized reception ($\Delta = 0$, $\omega_o = 0$). Fig. 9 (dashed lines) shows the evolution of $\mathcal{P}_\epsilon^*$ as a function of the E_s/N_0 for several values of R_c (from right $R_c = 3/5$ to left $R_c = 1/3$), over the Galois Field order $q = 64$.

Moreover, the solid curves in Fig. 9 represents the probability of error $\mathcal{P}_\epsilon$ obtained with the GF(2^6)-LDPC code

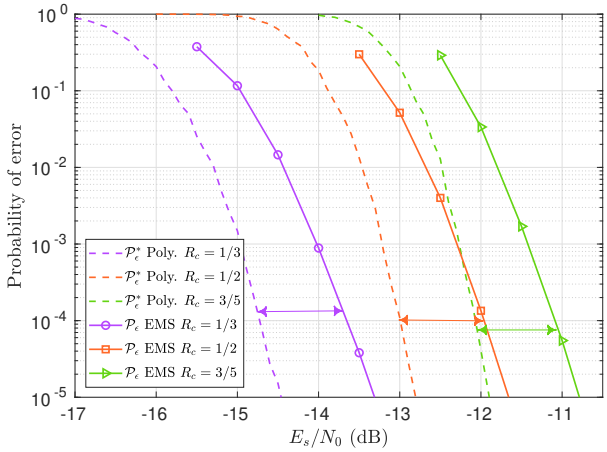

Fig. 9: $\mathcal{P}_\epsilon$, Polyanski and NB-LDPC (EMS over GF(64)) for QCSP Frame of $N = 120$ symbols, and different values of code rate R_c.

as defined in [36] for the same parameters. The decoding algorithm used is the Extended Mean Sum (EMS) with 30 decoding iterations and $n_m = 20$ (see [37] for the definition of the EMS algorithm and the Parity check matrix being used).

2) Detection-Correction trade-off: At very low SNRs, the successful transmission of short frames, as targeted by the NB-code and CCSK association in the QCSP system, is a challenging problem. In fact, the overall joint probability of successful transmission in an asynchronous ALOHA system can be expressed as $\mathcal{P} = \mathcal{P}_d \times \mathcal{P}_s \times \mathcal{P}_c$, where $\mathcal{P}_d$ is the probability of detection of the frame, $\mathcal{P}_s$ is the probability of correct estimation of the time-synchronization parameters, and $\mathcal{P}_c$ is the probability of correction of all transmission errors by the NB-code. Aiming to maximize the probability of successful transmission, we must maximize the probability of detection, synchronization, and decoding. For more clarification, Frame Error Rate (FER) is defined as

$$\text{FER} = \mathcal{P}_{\text{md}} + (1 - \mathcal{P}_{\text{md}})\mathcal{P}_{\text{ms}} + (1 - \mathcal{P}_{\text{md}})(1 - \mathcal{P}_{\text{ms}})\mathcal{P}_\epsilon, \tag{39}$$

where $\mathcal{P}_{\text{md}}$, $\mathcal{P}_{\text{ms}}$ and $\mathcal{P}_\epsilon$ are the miss detection, miss synchronization and error in correction probabilities respectively.

In order to give a better illustration, a practical case study is given in Fig. 10 that shows the simulation results of the FER of a QCSP frame of $N = 120$ symbols and $q = 64$, in both synchronous and asynchronous complex AWGN channels. FER is considered as the joint effect of miss detection and decoding error probability through a MC simulation. The threshold value U_0 is chosen corresponding to $\mathcal{P}_{\text{fa}} = 10^{-6}$. According to the earlier discussion on detection performance in section II-C, in the asynchronous channel, we choose to limit the deviation to $q/16 = 4$ chips and the frequency offset to $\omega_o = \pi/4$ at the receiver side. This is achieved by adjusting the bin size appropriately to $(\omega_b = \pi/2, \ell = q/8)$ for uniformly distributed random frequency and time offsets. For the decoding performance, we assume that the synchronization parameters can be perfectly found after the detection process. Note that the time and phase synchronization protocols are studied and illustrated

in [38], [39]. It is worth noticing here that the MC simulations of the whole system give performances that matches (39), considering the synchronization process after the detection is perfect ($\mathcal{P}_{\text{ms}} = 0$), i.e. FER $= \mathcal{P}_{\text{md}} + (1 - \mathcal{P}_{\text{md}})\mathcal{P}_{\epsilon}$.

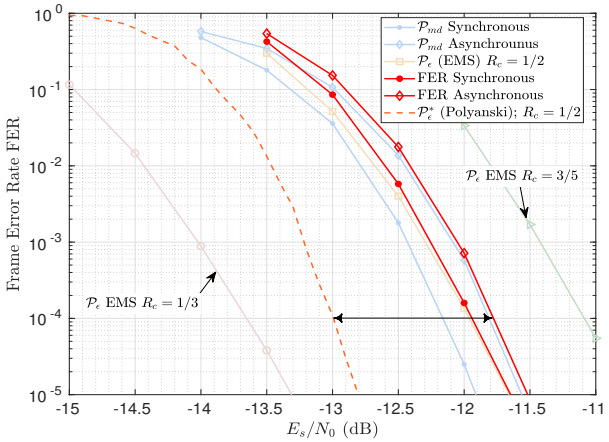

Fig. 10: Joint FER due to $\mathcal{P}_{\epsilon}$, $\mathcal{P}_{\text{md}}$ and to $\mathcal{P}_{\text{fa}} = 10^{-6}$ for $N = 120$ symbols, where $R_c = 1/2$, in synchronous and asynchronous complex AWGN channel.

As can be seen, the gap between the simulated FERs and the Polyanskiy's bound is around 1.2 dB, i.e., FER $= 10^{-4}$ at $E_s/N_0 = -11.80$ dB. Note also here that using an EMS decoder of a code rate $R_c = 1/3$ is useless since the system will have an over-coding performance with an overall FER performance curves highly impacted by the detection performance $\mathcal{P}_{\text{md}}$. Also, if the system uses an EMS decoder of a coding rate in this case of $R_c = 3/5$, we will obtain an over-detection performance, with a FER performance highly impacted by the decoding performance $\mathcal{P}_{\epsilon}$. For this reason, we have chosen $R_c = 1/2$ as an appropriate rate for the NB-code in the aforementioned scenario.

So for a given E_s/N_0 and a given payload, finding the optimal QCSP structure (code rate, q size) that minimizes FER for a given receiver complexity is still an open problem for obtaining the best detection-correction (and further synchronization) trade-off.

E. A comparison with a classical preamble-based frame

In this section we will use the QCSP results obtained in the previous section for $K = 60$ symbols, i.e., $m = 360$ bits of payload, and $R_c = 1/2$ for the comparison. To do this comparison with up-to-date codes, we build an adhoc solution taking elements from the 5G-LDPC 3rd Generation Partnership Project (3GPP) standard in a synchronized channel. The preamble is composed of a length $p = 793$ symbols thanks to Zadoff–Chu sequence. This is the minimum length required to guarantee a probability of misdetection of 10^{-4} with a probability of false alarm of 10^{-6} at E_s/N_0 of -11.95 dB (result obtained by MC simulation with a fully synchronized preamble, i.e., with perfect time synchronization ($\Delta = 0, f_o = 0$)). For the error correction scheme, the LDPC code, with rate $1/3$ and $k = 360$, of the 3GPP standard is used. This code requires a E_s/N_0 of 0.2 dB to obtain a FER of 10^{-4} [40]. The transmission of 17 repetitions of encoded frame gives a FER 10^{-4} at E_s/N_0 of $0.2 - 10\log_{10}(17) = -12.10$ dB. The encoded frame is thus of size $\frac{360}{2} \times 3 \times 17 = 9180$ QPSK symbols. Subsequently, the total frame length with a classical solution should be equal to $793 + 9180 = 9973$ symbols. To summarize, the size of the QCSP sequence is 7680 ($60 \times 2 \times 64$), while a frame with the classical method requires 9973 symbols. Thus, using the QCSP scheme, the frame size is reduced by 22.98% $\approx$ 23% as shown in the schematic of Fig. 11. This 23% translates directly into an increase of the wireless channel capacity and in energy saving for the wireless sensors.

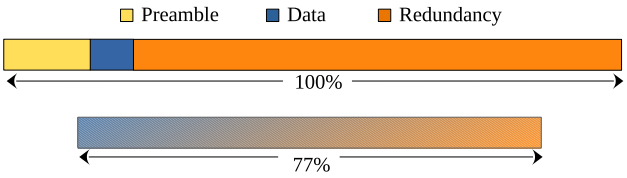

Fig. 11: Classical vs. preamble-less proposed approach (QCSP) for transmitting a frame.

Moreover, it is worth mentioning that the QCSP frame has an additional significant advantage compared to the classical frame: the length of the CCSK sequences is 64, whereas the length of the preamble is 793. This implies that the preamble's based frame is $793/64 = 12.39$ more sensitive to a frequency offset than the QCSP frame. This ratio of sensitivity is translated directly into the number of parallel filters (frequency bin size ω_b in the time-frequency grid decomposition) required to test the different frequency offset hypotheses.

VI. Conclusion

The paper proposes a new frame structure called Quasi-Cyclic Short Packet for the transmission of short packets in a LPWAN. The QCSP frame relies on the combination of CCSK modulation and non-binary error control codes. The whole frame can be considered either as a preamble sequence to perform detection and synchronization, or as a noisy codeword to perform the non-binary error correcting process. Owing to this structure, the QCSP frame offers the capability of blind detection and self-synchronization without any additional overhead knowing that in this article we didn't discuss the self-synchronization aspect.

A formal performance model of the frame detection algorithm has been first derived, then empirically verified by a MC simulation. Consequently, an analysis of the frame detection algorithm has been studied where it gives insight on the impact of each parameter on the detection performance according to the QCSP frame structure (size and GF order), the time and frequency offsets. The trade-off between detection and error-correction performance has been presented. As a case study, it is shown that a QCSP frame over GF(64) with $N = 120$ symbols can be received (detected and decoded) correctly with a frame error rate of 10^{-4} at an E_s/N_0 less than 1.2 dB from Polyanskiy bound. Finally, a comparative example

between the proposed QCSP and a classical preamble-based frame (Zadoff-Chu sequence-based preamble and the LDPC error correction code being used in the 3GPP (5G) standard) has been considered. We have shown that, at the same level of performance, the QCSP frame length is approximately 23% smaller than the classical preamble-based frame. This frame reduction can be translated into an increase in the wireless channel capacity, and the saving of the wireless sensors power consumption.

The study is going to be extended in several directions. First, the synchronization process as well as its impact on the performance will be studied and evaluated. Second, the discussion of the Detection-Correction approach in section V-D2 opens an interesting theoretical question regarding the optimal frame structure to fulfil the requirement of an application with the minimum energy cost at the transmission side. Finally, the paper deals only with the AWGN channel; future work is going to extend the investigation to multi-path channels and in the context of IoT multi user access.

To conclude, we believe that the QCSP scheme can be useful in many applications. It could compete with existing solutions such as LoRA, Sigfox and NB-LTE solutions in a LPWAN. It could be also used to establish a communication link in an ALOHA protocol between a terminal and a communication infrastructure (constellation of low earth orbital satellites, base station of a mobile network, etc.).

ACKNOWLEDGMENT

The research leading to these results received funding from the French National Research Agency ANR-19-CE25-0013-01 part of the project QCSP (website: https://qcsp.univ-ubs.fr/).

REFERENCES

[1] K. Mekki, E. Bajic, F. Chaxel, and F. Meyer, "A comparative study of LPWAN technologies for large-scale IoT deployment," vol. 5, pp. 1–7, March 2019.

[2] U. Raza, P. Kulkarni, and M. Sooriyabandara, "Low Power Wide Area Networks: An Overview," *IEEE Communications Surveys Tutorials*, vol. 19, no. 2, pp. 855–873, 2017.

[3] I. F. Akyildiz, Weilian Su, Y. Sankarasubramaniam, and E. Cayirci, "A survey on sensor networks," *IEEE Communications Magazine*, vol. 40, no. 8, pp. 102–114, 2002.

[4] R. Ratasuk, B. Vejlgaard, N. Mangalvedhe, and A. Ghosh, "NB-IoT system for M2M communication," in *2016 IEEE Wireless Communications and Networking Conference Workshops (WCNCW)*, 2016, pp. 428–432.

[5] Y. E. Wang, X. Lin, A. Adhikary, A. Grovlen, Y. Sui, Y. Blankenship, J. Bergman, and H. S. Razaghi, "A Primer on 3GPP Narrowband Internet of Things," *IEEE Communications Magazine*, vol. 55, no. 3, pp. 117–123, 2017.

[6] C. Berrou, A. Glavieux, and P. Thitimajshima, "Near Shannon limit error-correcting coding and decoding: Turbo-codes. 1," in *Proceedings of ICC '93 - IEEE International Conference on Communications*, vol. 2, 1993, pp. 1064–1070 vol.2.

[7] Lora-Alliance. LoRaWAN TM 101 A Technical Introduction. Technical Marketing Workgroup 1.0, November 2015. [Online]. Available: http://www.lora-alliance.org

[8] Lavric, Alexandru and Petrariu, Adrian I. and Popa, Valentin, "Long Range SigFox Communication Protocol Scalability Analysis Under Large-Scale, High-Density Conditions," *IEEE Access*, vol. 7, pp. 35 816–35 825, 2019.

[9] G. Durisi, T. Koch, and P. Popovski, "Toward Massive, Ultrareliable, and Low-Latency Wireless Communication With Short Packets," *Proceedings of the IEEE*, vol. 104, no. 9, pp. 1711–1726, Sep. 2016.

[10] Y. Polyanskiy, "Asynchronous Communication: Exact Synchronization, Universality, and Dispersion," *IEEE Transactions on Information Theory*, vol. 59, no. 3, pp. 1256–1270, March 2013.

[11] S. Kim, K. Joo, and Y. Lim, "A delay-robust random access preamble detection algorithm for LTE system," in *2012 IEEE Radio and Wireless Symposium*, 2012, pp. 75–78.

[12] Z. Ye, C. Duan, P. V. Orlik, J. Zhang, and A. A. Abouzeid, "A Synchronization Design for UWB-Based Wireless Multimedia Systems," *IEEE Transactions on Broadcasting*, vol. 56, no. 2, pp. 211–225, 2010.

[13] T. M. Schmidl and D. C. Cox, "Robust frequency and timing synchronization for OFDM," *IEEE Transactions on Communications*, vol. 45, no. 12, pp. 1613–1621, 1997.

[14] D. Zhu and R. W. Heath, "Directional timing synchronization in wideband millimeter wave cellular systems with low-resolution ADCs," in *2017 51st Asilomar Conference on Signals, Systems, and Computers*, 2017, pp. 37–41.

[15] M. Schlüter, M. Dörpinghaus, and G. P. Fettweis, "Bounds on Phase, Frequency, and Timing Synchronization in Fully Digital Receivers With 1-bit Quantization and Oversampling," *IEEE Transactions on Communications*, vol. 68, no. 10, pp. 6499–6513, 2020.

[16] D. Godard, "Self-Recovering Equalization and Carrier Tracking in Two-Dimensional Data Communication Systems," *IEEE Trans. Commun.*, vol. 28, pp. 1867–1875, 1980.

[17] T. Fujita, D. Uchida, Y. Fujino, O. Kagami, and K. Watanabe, "A burst modulation/demodulation method for short-packet wireless communication systems," in *2008 14th Asia-Pacific Conference on Communications*, 2008, pp. 1–5.

[18] A. Azari, P. Popovski, G. Miao, and C. Stefanovic, "Grant-Free Radio Access for Short-Packet Communications over 5G Networks," in *GLOBECOM 2017 - 2017 IEEE Global Communications Conference*, 2017, pp. 1–7.

[19] B. Bloessl and F. Dressler, "mSync: Physical Layer Frame Synchronization Without Preamble Symbols," *IEEE Transactions on Mobile Computing*, vol. PP, pp. 1–1, 02 2018.

[20] P. Walk, P. Jung, B. Hassibi, and H. Jafarkhani, "MOCZ for Blind Short-Packet Communication: Practical Aspects," *IEEE Transactions on Wireless Communications*, vol. 19, no. 10, pp. 6675–6692, 2020.

[21] O. Abassi, L. Conde-Canencia, M. Mansour, and E. Boutillon, "Non-Binary Low-Density Parity-Check coded Cyclic Code-Shift Keying," in *2013 IEEE Wireless Communications and Networking Conference (WCNC)*, April 2013, pp. 3890–3894.

[22] A. Y. . Wong and V. C. M. Leung, "Code-phase-shift keying: a power and bandwidth efficient spread spectrum signaling technique for wireless local area network applications," in *CCECE '97. Canadian Conference on Electrical and Computer Engineering. Engineering Innovation: Voyage of Discovery. Conference Proceedings*, vol. 2, May 1997, pp. 478–481 vol.2.

[23] G. M. Dillard, M. Reuter, J. Zeiddler, and B. Zeidler, "Cyclic code shift keying: a low probability of intercept communication technique," *IEEE Transactions on Aerospace and Electronic Systems*, vol. 39, no. 3, pp. 786–798, July 2003.

[24] A. Voicila, D. Declercq, F. Verdier, M. Fossorier, and P. Urard, "Low-complexity decoding for non-binary LDPC codes in high order fields," *IEEE Transactions on Communications*, vol. 58, no. 5, pp. 1365–1375, May 2010.

[25] G. Liva, E. Paolini, B. Matuz, S. Scalise, and M. Chiani, "Short Turbo Codes over High Order Fields," *IEEE Transactions on Communications*, vol. 61, no. 6, pp. 2201–2211, June 2013.

[26] R. Zhou, R. Le Bidan, R. Pyndiah, and A. Goalic, "Low-Complexity High-Rate Reed-Solomon Block Turbo Codes," *IEEE Transactions on Communications*, vol. 55, no. 9, pp. 1656–1660, Sep. 2007.

[27] R. Mori and T. Tanaka, "Non-binary polar codes using Reed-Solomon codes and algebraic geometry codes," in *2010 IEEE Information Theory Workshop*, Aug 2010, pp. 1–5.

[28] S. Pfletschinger and D. Declercq, "Getting Closer to MIMO Capacity with Non-Binary Codes and Spatial Multiplexing," in *2010 IEEE Global Telecommunications Conference GLOBECOM 2010*, Dec 2010, pp. 1–5.

[29] Y. Polyanskiy, H. V. Poor, and S. Verdu, "Channel Coding Rate in the Finite Blocklength Regime," *IEEE Transactions on Information Theory*, vol. 56, no. 5, pp. 2307–2359, May 2010.

[30] M. Hyder and K. Mahata, "Zadoff–Chu Sequence Design for Random Access Initial Uplink Synchronization in LTE-Like Systems," *IEEE Transactions on Wireless Communications*, vol. 16, no. 1, pp. 503–511, 2017.

[31] Malik Muhammad Usman Gul, Sungeun Lee, and Xiaoli Ma, "Robust synchronization for OFDM employing Zadoff-Chu sequence," in *2012 46th Annual Conference on Information Sciences and Systems (CISS)*, 2012, pp. 1–6.

[32] E. Boutillon. ”PN Sequence Generation in QCSP systems”. [Online]. Available: https://qcsp.univ-ubs.fr/wp-content/uploads/2021/11/Sequence_PN.pdf
[33] V. Savin, “Non-binary polar codes for spread-spectrum modulations,” in *2021 11th International Symposium on Topics in Coding (ISTC)*, 2021.
[34] C. Monière, K. Saied, B. Legal, and E. Boutillon, “Time sliding window for the detection of CCSK frames,” in *accepted to the IEEE Workshop on Signal Processing Systems (SiPS’2021)*, 2021, pp. 1–6.
[35] N. C. Beaulieu, “An infinite series for the computation of the complementary probability distribution function of a sum of independent random variables and its application to the sum of Rayleigh random variables,” *IEEE Transactions on Communications*, vol. 38, no. 9, pp. 1463–1474, Sep. 1990.
[36] (2020) Web site on Non-Binary LDPC. [Online]. Available: http://www-labsticc.univ-ubs.fr/nb_ldpc/.
[37] E. Boutillon, L. Conde-Canencia, and A. Al Ghouwayel, “Design of a GF(64)-LDPC Decoder Based on the EMS Algorithm,” *IEEE Transactions on Circuits and Systems I: Regular Papers*, vol. 60, no. 10, pp. 2644–2656, Oct 2013.
[38] K. Saied, A. Ghouwayel, and E. Boutillon, “Time-Synchronization of CCSK Short Frames,” in *17th International Conference on Wireless and Mobile Computing, Networking and Communications (WiMob’2021)*, Bologna, Italy, Oct. 2021.
[39] K. Saied, A. Ghouwayel and E. Boutillon, “Phase Synchronization for NB-LDPC Coded CCSK Short Frames,” in *Submitted to the 2022 IEEE Vehicular Technology Conference (VTC2022)*.
[40] 3GPP, “Performance evaluation of LDPC codes for NR eMBB data,” 3rd Generation Partnership Project (3GPP), Discussion and decision R1-1713740, August 2017, version 6.1.4.1.6. [Online]. Available: https://www.3gpp.org/ftp/TSG_RAN/WG1_RL1/TSGR1_90/Docs/R1-1713740.zip

Kassem Saied received the Masters degree in Telecommunication Engineering from the Lebanese International University (LIU), Lebanon, in 2017. He then received the Research Masters degree in Signal, Telecom, Image, Speech Processing(STIP) from the Lebanese University (LU), Lebanon, in 2018. In March 2022, he finishes the Ph.D studies at the Université de Bretagne Sud, France at the Lab-STICC. He worked on the QCSP project funded from French National Research Agency ANR-19-CE25-0013-01 (https://qcsp.univ-ubs.fr/). His research activities are focused on proposing and studying new algorithms in the field of short packets transmission in wireless communications for the Internet of Things (IoT).

Ali Chamas Al Ghouwayel received his B.E. degree in Physics-Electronics in 2002 from the Lebanese University, Beirut, his B.E. degree in Electronics Engineering and his M.S. Degree in Telecommunications in 2004 from the National School of Engineering of Brest (ENIB), France, and his Ph.D. in Signal Processing and Telecommunications in 2008 from the High School of Electricity (Supélec) and University of Rennes 1, France. His research activities concerned Parametrization Study for Software Defined Radio Systems. In 2008, He joined the Lab-STICC laboratory in Lorient, France and worked as a Post-Doctoral researcher on the European Project DAVINCI. In 2010, He joined the Lebanese International University, in Beirut, Lebanon, as Assistant Professor and then promoted to the rank of Associate Professor in 2016. His current research interests include Study, Optimization, and Adequation Algorithm Architecture for Hardware Implementation of ultra-throughput Non-Binary LDPC decoders on FPGA and ASIC, Internet of Things (IoT) Frame detection and synchronization at very low SNR, and the investigation of new technologies and signaling techniques enabling the usage of the spectrum in the sub-THz bands 90GHz-200GHz. He has several refereed journal and conference papers. He also served as Reviewer for several IEEE Transactions Journals and TPC for IEEE Conferences. In August 2020, He joined the School of Engineering EFREI Paris as the Head of the Embedded Systems Division.

Emmanuel Boutillon received the Engineering Diploma in 1990 and its Ph.D. degree in 1995, both from the Telecom Paris Tech, Paris. From 1995 to 2000, he was an assistant professor in Telecom Paris Tech. In 1998, he spent a sabbatical year at the University of Toronto, Ontario, Canada. In 2000, he moved to the Université de Bretagne Sud (Lorient, France) as a professor. He headed the LESTER lab from 2005 up to the end of 2007. He was then head of CACS department (Lab-STICC) until 2016. In 2011, he had a sabbatical year at INICTEL-UNI, Lima (Peru). His research interests are on the interactions between algorithm and architecture in the field of wireless communications and high speed signal processing. In particular, he works on binary and nonbinary decoders.